




Phononic transport and simulations of annealing processes in nanometric complex structures

Alberto Sciuto ^{1,2} Ioannis Deretzis,¹ Giuseppe Fiscaro,¹ Salvatore Francesco Lombardo,¹ Maria Grazia Grimaldi,² Karim Huet,³ Benoit Curvers ³ Bobby Lespinasse,³ Armand Verstraete,³ and Antonino La Magna ^{1,*}

¹*CNR-IMM, Z.I. VIII Strada 5, I-95121 Catania, Italy*

²*Dipartimento di Fisica e Astronomia, Università di Catania, Via S. Sofia 64, 95123 Catania, Italy*

³*Laser Systems and Solutions of Europe (LASSE), 14-38 Rue Alexandre, 92230 Gennevilleres, France*



(Received 14 August 2019; accepted 22 April 2020; published 22 May 2020)

Modeling thermal transport at the nanoscale is a difficult task, especially when external time-varying heating sources and the complexity of the studied systems make computational schemes that rely on accurate particlelike simulations nonaffordable. Alternative strategies based on corrections of the Fourier law could satisfy the trade-off between accuracy and computational efficiency, since they can be implemented in partial differential equation solvers. This continuum approach could also allow for the coupling between thermal transport and other evolving fields related to the generalized temperature field. Here we demonstrate that corrections due to the finite phonon mean free paths can be suitably included in annealing process simulations of three-dimensional nanosystems. Quantitative predictions can be obtained and readily compared with the experimental characterization of the processed samples.

DOI: [10.1103/PhysRevMaterials.4.056007](https://doi.org/10.1103/PhysRevMaterials.4.056007)

I. INTRODUCTION

The release of energy towards a processed sample is probably one of the most important aspects of material manipulation processes. Temperature control, heating, annealing, and quenching are mandatory keywords of any sample preparation method in the scientific literature. Often, when standard laboratory practices for macroscopic samples are directly applied to the manufacturing of nanoscale systems, they become critical. If, in addition to the system size, also the process time shrinks (as in the case of laser thermal annealing (LTA) with nanosecond range pulses [1]), the critical issues become huge and the accurate process control requires basic research also supported by reliable modeling. An accurate theoretical approach of heat transport at the nanoscale relies either on direct solutions of the Boltzmann transport equation (BTE) for phonons [2] or on atomistic simulations in the molecular dynamics framework [3]. These methods are fundamental for achieving a deep understanding of the energy transport in particular nanosystems, but their application could be too cumbersome when applied in a thermal process simulation.

Indeed, an advanced simulation of a thermal process (including a laser process) aims at predicting the modifications of a material presumably in the presence of complex structures (e.g., with nanometer-wide elements made of different materials and/or phases and in thermal contact with meso- and macroscopic objects like substrates, supports, etc.). Moreover, it is generally a multiphysics problem where several “fields” [4–12] (i.e., electromagnetic field, impurity density, local time-dependent phases, etc.) self-consistently interact with the temperature field. In this framework, heat transport is usually

modeled by means of numerical solutions of the Fourier law (FL), expressed as a partial differential equation (PDE), by means of the finite element method (FEM), or similar numerical schemes, when suitable space-time-dependent heat sources and boundary conditions are defined.

Such an approach shows strong limitations for nanoscale systems with complex boundaries and material specifications, where, e.g., the regime of transport for phonons can change from diffusive to ballistic. As a consequence, an appealing improvement of the heat transport model for structures with component sizes comparable to their intrinsic phonon mean free paths should maintain this continuum description in order to allow for a direct integration in process simulators while introducing a proper formulation for the corrections due to the phonons’ dynamics. Advancements in this sense appear in the recent literature [13,14], where the important general conclusion is that corrections due to the finite size of the system are based on Fourier law-like PDEs (where the thermal conductivity is the only material-dependent parameter in the bulk), whereas boundary conditions (BCs) of the corrections have to be significantly modified in order to consider the transport of phonons. In this context, we have integrated phonon transport corrections to our existing simulation tool LIAB (LASSE Innovation Application Booster [15]) in order to reproduce experimental data and predict the behavior of various material structures upon thermal annealing, including laser annealing [16]. Our continuum modeling is thus integrated in a FEM framework and the corrections allow for achieving a calibrated method able to simulate thermal processes from the diffusive to the ballistic regime of phonon dynamics. Within this approach, we have simulated different cases where heating is induced by conventional and laser annealing in various complex bi- and tridimensional (2D and 3D) structures. Results are in excellent agreement with the experiments and demonstrate that a continuous treatment of

*antonino.lamagna@imm.cnr.it

thermal transport is possible in complex nanosize systems in thermal contact with macroscopic objects.

II. HEAT TRANSPORT MODEL

The Fourier law can be expressed as

$$\vec{F}_Q = -k\nabla T, \quad (1)$$

where F_Q is the net heat flux, k is the thermal conductivity, and T is the temperature. Equation (1) is ubiquitously applied for the study of heat diffusion problems and it can be formally derived from the BTE for local phonon distributions close to the thermodynamic equilibrium, assuming the continuum limit and the diffusive regime [17]. Recently [14] a systematic expansion in terms of continuum quasithermal fields has been derived, indicating that the FL is the correct zero-order approximation for the phononic BTE in the (diffusive) limit of a small Knudsen number $\langle \text{Kn} \rangle$. We notice that $\langle \text{Kn} \rangle$ is a dimensionless number defined as the ratio between the average phonons' mean free path and the representative length of the system in study. In the diffusive approximation, the same derivation [14] demonstrates that the usual (1) Dirichlet ($T = T_0$), (2) Neumann ($\nabla T = 0$), and (3) continuity ($-k^1 \nabla T_1|_\Gamma = -k^2 \nabla T_2|_\Gamma$ and $T_1|_\Gamma = T_2|_\Gamma = T$) relations are the correct boundary conditions, respectively, for (1) the thermostat at temperature T_0 , (2) the diffusely specular wall, and (3) the interface Γ between two materials 1 and 2 with thermal conductivities k^1 and k^2 . The analysis of high-order corrections in $\langle \text{Kn} \rangle$ shows that these are ruled by FL-type equations in the bulk (all ruled by the bulk conductivity), whereas boundary conditions have to be modified with jump-type BCs for the temperature [14]. Interesting analytic results in simple one-dimensional systems [13] show that by using the FL and suitable jump BCs, we can obtain exact solutions in the diffusive $\langle \text{Kn} \rangle \ll 1$ and ballistic $\langle \text{Kn} \rangle \gg 1$ limits, while the solutions deviate only a few percent with respect to the BTE solution in the intermediate $\langle \text{Kn} \rangle \sim 1$ region. If we consider a system in contact with a thermostat at a temperature T_0 , the jump boundary conditions can be written as

$$\hat{n} \cdot \vec{F}_Q = k_{\text{bulk}} \lambda^{-1} (T - T_0), \quad (2)$$

where $\vec{F}_Q = \vec{F}_Q^+ - \vec{F}_Q^-$ is the combined phonon flux coming from the left and right sides of the junction between the nanosystem and the thermostat, k_{bulk} is the bulk thermal conductivity of the material, and λ is the average phonon scattering length, which can be related to known and measurable material properties as

$$\lambda(T) = 4k_{\text{bulk}}(T)/C(T)v_s(T), \quad (3)$$

where $v_s(T)$ is the sound velocity and $C(T)$ is the thermal capacitance, which is also used in the time-dependent bulk equation for the T field

$$C(T) \frac{\partial T}{\partial t} = \nabla \cdot [k_{\text{bulk}}(T) \nabla T] + S(t), \quad (4)$$

with $S(t)$ the eventual time-dependent internal source. Equation (4) is numerically solved in the simulation results of Sec. IV.

We note that the interpolating boundary correction [Eq. (3)] derives from a multiple-temperature approach to the

local nonequilibrium, due to ballistic effects. T is the average temperature [13] and the multiple temperature collapses to a single T in the diffusive limit. If the system is significantly smaller than λ (ballistic limit, $\langle \text{Kn} \rangle \ll 1$) the corrected BCs in Eq. (2) impose that the phonon modes which are in thermal equilibrium with the thermostat at T_0 and at the interface do not thermalize with inner phonon modes: they reproduce correctly the behavior in the ballistic regime (details are discussed in Ref. [13]).

Extending this derivation with arguments coming from the Chapman-Enskog-like expansion of Ref. [14], we have to consider again the jump solutions at different temperatures T_1 and T_2 at the interface between two regions made of different materials. Consistent with the interpolating correction at the thermostat surface [Eq. (2)], the discontinuous solutions at the material's boundary Γ are

$$-k_{\text{bulk}}^1 \nabla T_1 = \hat{\Pi} (T_1|_\Gamma^+ \hat{n}_1 + T_2|_\Gamma^- \hat{n}_2), \quad (5)$$

where $\hat{n}_1 = -\hat{n}_2$ are the local outward normal unit vectors to the two sides of the boundary and $\hat{\Pi} = (k_{\text{bulk}}^1 \lambda_1^{-1} + k_{\text{bulk}}^2 \lambda_2^{-1})|_\Gamma$ is the local phonon-scattering functional. Moreover, the energy conservation condition at the boundary has to be imposed as [14]

$$-k_{\text{bulk}}^1 \nabla T_1|_\Gamma = -k_{\text{bulk}}^2 \nabla T_2|_\Gamma. \quad (6)$$

Equation (6) acts as a closure of the model at the interface location. We note that an external boundary simulating a virtual interface with the same material is still ruled by the Neumann relation $\nabla T = 0$. In the following we discuss the impact of the thermal mode equations introduced here [Eqs. (2)–(6)] by comparing corrected and standard solutions (i.e., solutions with strictly diffusive BCs) in the heating processes of 2D and 3D systems.

III. EFFECTIVE CONDUCTIVITY ANALYSIS

We start our analysis with Si nanowires (NWs) having their equilibrium shape [18] (i.e., an almost regular polygon with 12 edges) and different diameters. These are in contact with one or two thermostats along one or two perimeter edges, while internally heated by a uniform source. The effective phonon-scattering length λ is the only physical quantity of the model, which, in all the results presented in this paper, has been calibrated using the experimental values of $k_{\text{bulk}}(T)$, $C(T)$, and $v_s(T)$ which can also depend on T . In Fig. 1(a) we report a cross section, perpendicular to the Si NW axis, of the thermal field obtained for the standard Dirichlet BC(s) (left side) and the corrected BC(s) expression (right side) for the edge(s) in contact with the thermostat. The temperature obtained in the two cases along the NW diameter connecting the center of the thermostat edge and the opposite edge is shown in Fig. 1(b). For the thermal calibration of Si we used values deriving from Ref. [15] while the sound of speed was set to $v_s = 6400$ m/s [19]. In the simulations of single Si NWs (Figs. 1 and 2) the internal source is tuned in order to obtain an increase of the order of ~ 1 K for the internal temperature with respect to the thermostat. The difference between the standard and the corrected solution is relevant for this structure and it tends to enlarge (decrease) for smaller (larger) NWs (see also Sec. S1 of the Supplemental Material [20]).

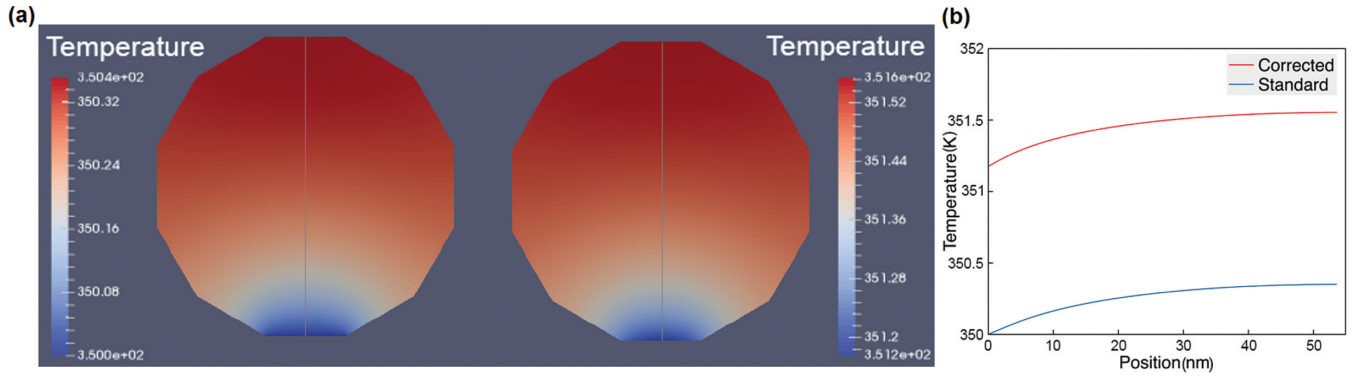


FIG. 1. (a) Cross section of a heated Si nanowire with a diameter of 56 nm: standard (left) and corrected (right) solutions. (b) Standard and corrected T values along the nanowire diameter line shown in (a).

Si NWs are reference systems for the study of phononic energy transport and they have been subjected to extensive experimental analyses. The interest in Si NWs has intensified from the apparent scaling of the thermal conductivity with

the diameter of the NW, and several papers reported these evidences. As a consequence, our model predictions could in principle be compared also with the experimental results. As a matter of fact, measurements are based on the “FL equivalent” behavior of the system: they are dependent on the uniform heat source and they have to be correctly interpreted in terms of the real microscopic behavior.

A direct method to compare the experimental [21] and theoretical results uses the apparent conductivity, k_{app} , concept [13]. k_{app} is a geometry-dependent parameter which describes a thermal field distribution T obtained in real and numerical experiments, assuming that the constitutive equation of T is the standard FL. As a consequence $k_{app} \simeq k_{bulk}$ in large systems while in the nanoscale its geometrical dependence includes also the real or virtual realization of the thermal contacts with the environment (e.g., the experimental apparatus). Following Ref. [13] we have calculated k_{app} with the results of our NW simulations as

$$k_{app}(T) = k_{bulk}(T) \frac{\langle T_{standard} - T_0 \rangle}{\langle T_{corrected} - T_0 \rangle}, \quad (7)$$

where $T_{correct}$ and $T_{standard}$ are the corrected and diffusive temperature fields evaluated numerically; the symbol T_0 is the thermostat temperature while $\langle \rangle$ indicates the average of the field expression over the space region occupied by the structures. The approximate estimates of k_{app} have been compared in Ref. [13] with direct Monte Carlo solutions of the Boltzmann transport for the thin-film geometry. The discrepancies between the two methods are globally below 6% and tend to zero in the ballistic and diffusive limits. Similar deviance could be expected if the continuum method is compared to accurate predictions based on the phonon mean-free-path sampling approach of Ref. [22].

In Fig. 2(a) the apparent conductivity $k_{app}(T)$, evaluated in a broad temperature range for Si NWs of different sizes and in the cases of the two types of thermal contacts, is compared with the $k_{bulk}(T)$ of bulk Si. We notice that the investigated temperature range starts at 200 K since at lower temperatures the phonon quantization makes our continuum analysis unfeasible. $k_{app}(T)$ is close to the bulk value for mesostructures in the micrometer range, while there is an important average reduction of $k_{app}(T)$ and a strong geometric effect for sizes of the order of ~ 100 nm and below. Consistently, we note that the quantitative value $k_{app}(T)$ significantly depends on

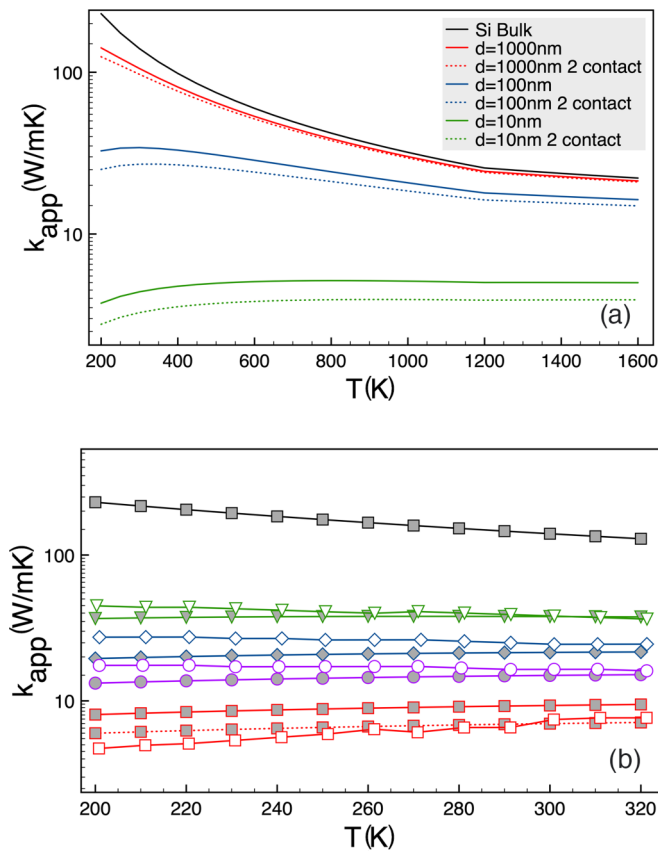


FIG. 2. (a) Evaluation of the apparent thermal conductivity for Si NWs with one and two thermal contacts and different sizes: 10 nm (green lines), 100 nm (blue lines), and 1000 nm (red lines). Bulk Si thermal conductivity is shown as a black line. (b) Comparison of simulated (solid grey markers, plain line for one contact, dotted for two contacts) and observed (open markers) thermal conductivity for Si NWs with different sizes: 22 nm (red lines), 37 nm (purple lines), 56 nm (blue lines), and 115 nm (green lines). Bulk Si thermal conductivity is shown as a black line. Experimental data extracted from Ref. [21].

the contact realization procedure at the nanoscale, while this dependence is less important at the mesoscale.

Our theoretical estimates of $k_{\text{app}}(T)$ can be compared with experimental measurements of the thermal conductivity, since any procedure of conductivity measurement implicitly uses the FL for the data analysis (i.e., we could reliably assume that experiments measure the apparent conductivity $k_{\text{app}}(T)$ of the nanosystem in a given configuration of the contacts). These comparisons are shown in Fig. 2(b), where experimental data (open symbols) are extracted by the data discussed in Ref. [21] while the numerical evaluations of $k_{\text{app}}(T)$ are plotted for single (solid lines) and double (dashed lines) contacts. Considering the numerous effects that can impact this analysis (e.g., the heat sources and the realization of the thermal contacts, the difference between real and ideal NW edges, the uniformity of the size along the NW axis, etc.), the agreement between calculations and measurements is noteworthy. Finally, we notice that the differences in the calculations of $k_{\text{app}}(T)$ for the single and double contacts and fixed size should have a counterpart in the experimental measurements, if the same nanosystem is studied with different measurement techniques or procedures.

IV. SIMULATIONS OF COMPLEX SYSTEMS

The demonstration of the reliability of the approach based on jump solutions for the heat transport equation opens perspectives for its application in the simulation of the annealing process of complex nanosystems. However, although the formal extension of the method is rather straightforward, its numerical implementation is more difficult due to the possible presence of solution discontinuities at the boundaries of the material. We have implemented the discontinuous Galerkin FEM approach in the time-dependent LIAB solver (see Sec. S2 of the Supplemental Material [20]) in order to numerically address this issue. In the following, we present some examples of laser annealing process simulations in complex nanosystems where the conventional and corrected solutions are compared.

The first system [see Fig. 3(a), where the used computational mesh is shown] is composed of a Ge telescopic NW (10 nm + 15 nm diameters) immersed in air and deposited over a Si substrate. In this geometry a thermal contact forms between the substrate and the larger portion of the telescopic NW. The used value of the speed of sound in Ge is $v_s = 5400$ m/s [24], while the interface with the air is ruled by an effective value of $\lambda_{\text{air}} = 3$ nm (see also Ref. [20] for a discussion on the effect of this parameter). The calibration of the thermal parameters for Ge is that reported in Ref. [23] (being also the default calibration in LIAB). LIAB implements a self-consistent solution of laser annealing, where the heat source [see Fig. 3(b) for the source distribution of a transverse electric incident wave] is evaluated by means of the solution of the Maxwell equations in the time-harmonic approximation, once the temperature field is known [15]. In our simulation, we use the same laser pulse setting (wavelength 308 nm, pulse width ~ 160 ns; see Sec. S3 of the Supplemental Material [20]) of Ref. [15] and a fixed energy density of 0.4 J/cm².

The solutions (corrected and standard) of the thermal field distribution along the NW axis obtained after 5 ns of simulated

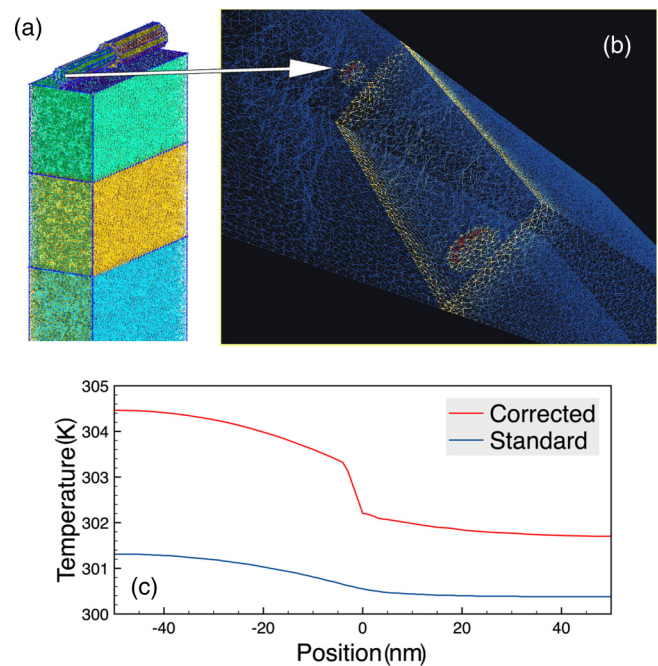


FIG. 3. (a) Computer-aided design (CAD) model and mesh of a Ge telescopic NW on a Si substrate: the colors distinguish the different elements used to compose the CAD geometry. (b) Heat source distribution mapped in the structure mesh used for FEM calculations. The arrow indicates equivalent regions in (a) and (b). (c) Comparison of thermal profiles obtained after 5 ns of simulated LTA using standard and corrected BCs.

annealing are shown in Fig. 3(b). The different temperatures (blue lines) obtained in the two sides of the junction when the standard FL rules the transport are due to a combined effect of different sizes and the differently absorbed heat. However, the solution is obviously smooth along the NW junction axis. A completely different heat distribution is calculated for the corrected solution. Apart from the different average values of the temperature that are caused by overall reduced heat dissipation when phononic corrections are included at the nanoscale (confirmed by the previous analysis of the apparent conductivity), we can also observe an abrupt change of the temperature at the junction of the telescopic NW. We note that no contact resistance correction has been added in the heat transport model at the junction position, since the junction is not a material boundary, and this jump is caused only by the different types of BCs, considering a finite scattering length for the phonons at the material interfaces (the larger NW only forms a thermal contact with the Si substrate).

LTA has a great application potential for microelectronics and, as a consequence, we have tested our method considering the complex structure of a fin-shaped field effect transistor (FinFET). The simulation of the LTA process with the FL of heat diffusion for a Si fin partially embedded in a SiO₂ layer and a tungsten (W) gate [see Fig. 4(a)] has been extensively discussed in Ref. [15]. The used mesh is shown in Fig. 4(a) while the heat source distribution evaluated with the corrected model after 5 ns is shown in Fig. 4(b) (laser energy density of 0.4 J/cm²). For the phononic correction parameter we used $v_s = 5600$ [25] and $v_s = 5200$ m/s [24] in the SiO₂ and W

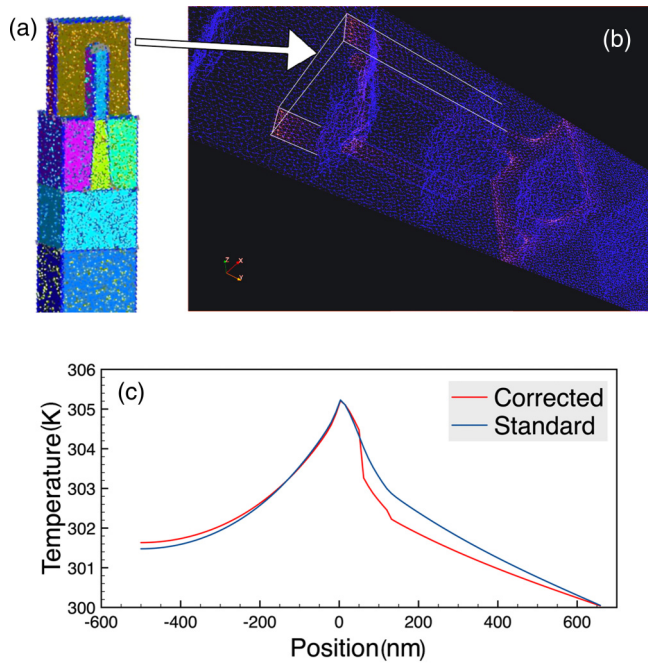


FIG. 4. (a) CAD model and mesh of a Si-gated FinFET structure. The colours distinguish the different elements used to compose the CAD geometry. (b) Heat source distribution mapped in the structure mesh used for FEM calculations. The arrow indicates equivalent regions in (a) and (b). (c) Comparison of thermal profiles obtained after 5 ns of simulated LTA using standard and corrected BCs.

regions, respectively. A comparison between the temperature field obtained with both the FL and the corrected model along a symmetric axis passing through the fin center demonstrates that corrections are necessary for an accurate simulation, although the differences are not so strong as in the telescopic NW case. As discussed previously, the modified geometric constraints can explain this reduced difference of the FL and corrected solutions: (a) the area of the cross section for the two nanosystems is different ($100/165 \text{ nm}^2$ for the NWs, $\sim 1000 \text{ nm}^2$ for the fin), (b) the boundary with the substrate is made of the same material for the fin, but of two different materials for the telescopic NW, and (c) only one side of the telescopic NW is in contact with the substrate, while the full fin is in contact with its own substrate.

V. CONCLUSION

To conclude, our investigation demonstrates that the inclusion of phononic corrections in the continuum heat transport

models is a feasible route for an accurate simulation of the heating processes of complex nanosystems. The goal of the method is the replacement of “*ad hoc*” geometric calibrations (e.g., the use of the size- and shape-dependent $k_{\text{app}}(T)$ in the FL) with a more experimentally or theoretically derived robust and general “material” calibration. In this work, we have explored the impact of a first-order phononic correction in simulations of heating for different 2D and 3D systems. This correction is able to interpolate between the diffusive and the ballistic regimes of thermal transport using as a single additional calibration parameter the average scattering length for the phonons in the material. The results of our numerical approach are promising: the corrections are important in the nanoscale; moreover, when comparisons with experiments are feasible, the solutions are able to recover the precise experimental scenario.

Limitations of the current method are related to the approximation of the phononic energy transport in terms of a single scalar average field and the consequent definition of a single phonon scattering length. Generalizations could be necessary in the cases where this approximation could be too stringent, as, e.g., in anisotropic materials, many phonon modes determine the heat conduction, or in the case of amorphous or disordered systems. The tensor form of the Fourier law is usually applied in anisotropic materials, which imposes a different formalization of the boundary relations [Eqs. (2)–(6)] in the framework of the present derivation. Our approach implicitly assumes the same average relaxation time for all phonon modes. Of course, the accurate inclusion of the relaxation term with respect to frequency and polarization shifts the problem to the BTE level. However, the qualitative framework of the present (approximate) derivation could be still useful also for disordered or amorphous materials or, in general, when heat transport is barely coupled with the sound transport mechanism. In this case, λ cannot be properly related to the material properties as in Eq. (3), but it should be considered as an *ad hoc* model parameter to be properly fitted. Finally, further refinements are possible, including additional corrections to the bulk constitutive equations, especially when atomically thin low-dimensional materials are considered (e.g., see Ref. [26]).

ACKNOWLEDGMENTS

I.D., G.F., and A.L. acknowledge that this project has received funding from the European Union’s Horizon 2020 research and innovation programme under Grant Agreement No. 871813 (MUNDFAB).

-
- [1] S. Lombardo, S. Boninelli, F. Cristiano, G. Fiscaro, G. Fortunato, M. Grimaldi, G. Impellizzeri, M. Italia, A. Marino, R. Milazzo, E. Napolitani, V. Privitera, and A. L. Magna, *Mater. Sci. Semicond. Process.* **62**, 80 (2017).
 - [2] J. Carrete, B. Vermeersch, A. Katre, A. van Roekeghem, T. Wang, G. K. Madsen, and N. Mingo, *Comput. Phys. Commun.* **220**, 351 (2017).
 - [3] X. Cartoixa, L. Colombo, and R. Rurali, *Nano Lett.* **15**, 8255 (2015).
 - [4] P. M. Fahey, P. B. Griffin, and J. D. Plummer, *Rev. Mod. Phys.* **61**, 289 (1989).
 - [5] P. A. Stolk, H.-J. Gossmann, D. J. Eaglesham, D. C. Jacobson, C. S. Rafferty, G. H. Gilmer, M. Jaraíz, J. M. Poate, H. S. Luftman, and T. E. Haynes, *J. Appl. Phys.* **81**, 6031 (1997).

- [6] A. A. Wheeler, W. J. Boettinger, and G. B. McFadden, *Phys. Rev. A* **45**, 7424 (1992).
- [7] N. A. Ahmad, A. A. Wheeler, W. J. Boettinger, and G. B. McFadden, *Phys. Rev. E* **58**, 3436 (1998).
- [8] M. Tabbal, M. J. Aziz, C. Madi, S. Charnvanichborikarn, J. S. Williams, and T. C. Christidis, *Proc. SPIE* **6458**, 645803 (2007).
- [9] A. La Magna, P. Alippi, V. Privitera, G. Fortunato, M. Camalleri, and B. Svensson, *J. Appl. Phys.* **95**, 4806 (2004).
- [10] A. La Magna, P. Alippi, V. Privitera, and G. Fortunato, *Appl. Phys. Lett.* **86**, 161905 (2005).
- [11] K. K. Ong, K. L. Pey, P. S. Lee, A. T. S. Wee, X. C. Wang, and Y. F. Chong, *Appl. Phys. Lett.* **89**, 172111 (2006).
- [12] G. Fiscaro, K. Huet, R. Negru, M. Hackenberg, P. Pichler, N. Taleb, and A. La Magna, *Phys. Rev. Lett.* **110**, 117801 (2013).
- [13] J. Kaiser, T. Feng, J. Maassen, X. Wang, X. Ruan, and M. Lundstrom, *J. Appl. Phys.* **121**, 044302 (2017).
- [14] J.-P. M. Péraud and N. G. Hadjiconstantinou, *Phys. Rev. B* **93**, 045424 (2016).
- [15] S. Lombardo, G. Fiscaro, I. Deretzis, A. L. Magna, B. Curvers, B. Lespinasse, and K. Huet, *Appl. Surf. Sci.* **467**, 666 (2019).
- [16] The specific sources of the code used for the calculations of the present paper can be released upon request to interested users.
- [17] N. Pottier, *Nonequilibrium Statistical Physics: Linear Irreversible Processes*, Oxford Graduate Texts (Oxford University Press, Oxford, 2010).
- [18] L. Vincent, R. Boukhicha, C. Gardès, C. Renard, V. Yam, F. Fossard, G. Patriarche, and D. Bouchier, *J. Mater. Sci.* **47**, 1609 (2012).
- [19] M. A. Hopcroft, W. D. Nix, and T. W. Kenny, *J. Microelectromech. Syst.* **19**, 229 (2010).
- [20] See Supplemental Material at <http://link.aps.org/supplemental/10.1103/PhysRevMaterials.4.056007> for deeper discussion on computational parameters and methods used.
- [21] J. Anaya, J. Jimenez, and T. Rodriguez, in *Nanowires*, edited by X. Peng (IntechOpen, Rijeka, 2012), Chap. 11.
- [22] A. J. H. McGaughey and A. Jain, *Appl. Phys. Lett.* **100**, 061911 (2012).
- [23] S. F. Lombardo, S. Boninelli, F. Cristiano, I. Deretzis, M. G. Grimaldi, K. Huet, E. Napolitani, and A. La Magna, *J. Appl. Phys.* **123**, 105105 (2018).
- [24] *Handbook of the Physicochemical Properties of the Elements*, edited by G. V. Samsonov (Springer, New York, 1968).
- [25] I. Zvára, *The Inorganic Radiochemistry of Heavy Elements* (Springer, Amsterdam, 2008).
- [26] P. Torres, F. Xavier Alvarez, X. Cartoixa, and R. Rurali, *2D Mater.* **6**, 035002 (2019).